Many-body localization: Transitions in spin models

John Schliemann,[1] João Vitor I. Costa,[2] Paul Wenk ●,[1] and J. Carlos Egues ●[2]

[1]*Institute for Theoretical Physics, University of Regensburg, Regensburg, Germany*
[2]*Instituto de Física de São Carlos, Universidade de São Paulo, 13560-970 São Carlos, São Paulo, Brazil*

We study the transitions between ergodic and many-body localized phases in spin systems, subject to quenched disorder, including the Heisenberg chain and the central spin model. In both cases systems with common spin lengths 1/2 and 1 are investigated via exact numerical diagonalization and random matrix techniques. Particular attention is paid to the sample-to-sample variance $(\Delta_s r)^2$ of the averaged consecutive-gap ratio $\langle r \rangle$ for different disorder realizations. For both types of systems and spin lengths we find a maximum in $\Delta_s r$ as a function of disorder strength, accompanied by an inflection point of $\langle r \rangle$, signaling the transition from ergodicity to many-body localization. The critical disorder strength is found to be somewhat smaller than the values reported in the recent literature. Further information about the transitions can be gained from the probability distribution of expectation values within a given disorder realization.

I. INTRODUCTION

Many-body localization has become in recent years one of the most intensively growing areas of research in condensed matter physics and beyond [1–8]. It denotes the absence of thermalization in an isolated interacting quantum system in the presence of typically strong disorder. In the opposite ergodic phase the eigenstate thermalization hypothesis is fulfilled stating that any appropriate subsystem of the isolated total system (being in a pure state) is accurately described by equilibrium statistical mechanics [9,10]. On the other hand, the presence of interactions distinguishes many-body localization from traditional Anderson localization [11,12].

In this work we revisit the transition from the ergodic to the many-body localized phase in disordered Heisenberg spin chains and compare it with the behavior of central spin models also subject to quenched disorder. For both types of systems we consider the spin lengths 1/2 and 1. We introduce a novel and very useful tool to quantify the transition, namely, the sample-to-sample variance of the averaged consecutive-gap ratio and the underlying probability distribution. As we will see in the following, a maximum of this variance signals, for both of the above systems and both spin lengths, the transition between ergodicity and many-body localization. This maximum is accompanied by an inflection point of of the averaged consecutive-gap ratio $\langle r \rangle$, suggesting a close analogy to classic phase transitions with $\langle r \rangle$ being an order parameter. These central observations are summarized in Figs. 2 and 7 for the Heisenberg chain and the central spin model, respectively.

An additional tool in the analysis of the transition from the ergodic to the many-body localized phase is the probability distribution of expectation values within a given disorder realization. The corresponding data is contained in Figs 5 and 9.

This paper is further organized as follows: In Sec. II we introduce the spin models to be studied and summarize the

underlying theoretical techniques. Our numerical results are presented in Sec. III, and we close with a summary and an outlook in Sec. IV.

II. MODEL AND APPROACH

A. Spin Hamiltonian

We study a periodic Heisenberg spin chain interacting with an additional central spin and being subject to a uniaxial quenched disorder field on each site of the chain,

$$H = J \sum_{i=1}^{K} \vec{I}_i \cdot \vec{I}_{i+1} + \frac{A}{K} \vec{S} \cdot \sum_{i=1}^{K} \vec{I}_i + 2S \sum_{i=1}^{K} h_i I_i^z, \quad (1)$$

where the parameter J describes the coupling of the K chain (or bath) spins $\vec{I}_i = \vec{I}_{i+K}$ to their nearest neighbors. The coupling to the central spin $\vec{S}$ is parametrized by A, and the random magnetic field h_i is chosen from a uniform distribution within the interval $[-h, h]$. In what follows all spins will have length $S = I = 1/2$ or $S = I = 1$.

For $S = I = 1/2$, the Hamiltonian (1) with $A = 0$, i.e., the Heisenberg spin-1/2 chain with quenched on-site disorder, is a workhorse of numerical studies of many-body localization [13–44]. The factor $2S$ in front of the disorder term makes contact to the usual parametrization for $S = 1/2$ and ensures an appropriate scaling behavior of the Hamiltonian for larger spin lengths. Specifically, when considering all spins as classical vectors of constant length (and not as operators), the transformation $S \mapsto qS$, $I \mapsto qI$ leads to $H \mapsto q^2 H$. Thus, disorder-induced effects on the dynamics should occur at the same disorder strength h. As we shall see in Sec. III, this remains approximately true when switching between $S = I = 1/2$ and $S = I = 1$.

Recent work by Hetterich *et al.* [45] studied the full model (1) for $S = I = 1/2$ concentrating on the case $J = 1$. As these authors argue, dividing the interaction parameter A by the

number of chain spins K, as done in Eq. (1), ensures that the spectral bandwidth of that coupling term is approximately independent of the system size. We will see in the following that this stipulation indeed has advantages when comparing data for different numbers of spins.

B. Random matrix theory

An important method to distinguish a many-body localized phase from an ergodic phase is random matrix theory, which is a theory for statistical fluctuations of energy levels of a given quantum system [46]. A modern tool to analyze the energy level statistics is the consecutive-gap ratio [47] defined as

$$r_n = \frac{\min\{s_n, s_{n-1}\}}{\max\{s_n, s_{n-1}\}} = \min\left\{\bar{r}_n, \frac{1}{\bar{r}_n}\right\}, \quad \bar{r}_n = \frac{s_n}{s_{n-1}}, \quad (2)$$

where $s_n = e_{n+1} - e_n$ is the difference between two neighboring energy levels e_{n+1}, e_n. In the strictly many-body localized (or integrable) phase, characterized by an extensive number of independent conserved quantities, the differences s_n obey Poisson statistics, and the probability distribution for the random variable $r = r_n$ can easily be determined to be [47]

$$p(r) = \frac{2}{(1+r)^2}. \quad (3)$$

On the other hand, in the fully ergodic phase, a system of the type (1) is generally assumed to be described by the Gaussian orthogonal ensemble (GOE) of random matrices [46]. Here the analysis of small random matrices mimicking the Hamiltonian predicts the pertaining probability distribution to be [48]

$$p(r) = \frac{27}{4} \frac{r + r^2}{(1 + r + r^2)^{5/2}}, \quad (4)$$

which can be seen as an analog of the classic Wigner surmises for probability distributions governing the traditional random variable $s = s_n$ [46].

As a consequence, the lowest moments of the probability distribution (3) in the integrable case are given by

$$\langle r \rangle_p = 2 \ln 2 - 1 \approx 0.3863, \quad (5)$$

$$\langle r^2 \rangle_p = 3 - 4 \ln 2 \approx 0.2274, \quad (6)$$

$$\Delta_p r = \sqrt{\langle r^2 \rangle_p - \langle r \rangle_p^2} \approx 0.2796, \quad (7)$$

with

$$\langle \cdot \rangle_p = \int_0^1 dr [p(r) \cdot], \quad (8)$$

whereas in the ergodic situation (4) we have

$$\langle r \rangle_p = 4 - 2\sqrt{3} \approx 0.5359, \quad (9)$$

$$\langle r^2 \rangle_p = \frac{27}{4} \ln\left(1 + \frac{2}{\sqrt{3}}\right) - \frac{1}{2} - \frac{5}{2}\sqrt{3} \approx 0.3515, \quad (10)$$

$$\Delta_p r \approx 0.2536. \quad (11)$$

C. Statistical data analysis

1. Disorder ensemble

Consider an ensemble of Q realizations of the local disorder field h_i, $i \in \{1, \ldots, K\}$. Each disorder realization, or sample, labeled by $\alpha \in \{1, \ldots, Q\}$ leads to a probability distribution $p_\alpha(r)$ for the consecutive-gap ratio $r \in [0, 1]$. Given an arbitrary function $f(r)$, these distributions determine the realization-dependent averages (or expectation values)

$$\langle f \rangle_\alpha = \int_0^1 dr \, p_\alpha(r) f(r) \quad (12)$$

with variances

$$(\Delta_\alpha f)^2 = \langle f^2 \rangle_\alpha - \langle f \rangle_\alpha^2. \quad (13)$$

The disorder-averaged probability distribution $p(r)$ *at given disorder strength* (and other system parameters) is

$$p(r) = \lim_{Q \to \infty} \frac{1}{Q} \sum_{\alpha=1}^{Q} p_\alpha(r), \quad (14)$$

and a good numerical estimate for this quantity is

$$p(r) \approx \frac{1}{Q} \sum_{\alpha=1}^{Q} p_\alpha(r), \quad Q \gg 1, \quad (15)$$

for sufficiently large Q. The disorder-averaged expectation values of $f(r)$ read

$$\langle f \rangle_p = \int_0^1 dr \, p(r) f(r) = \lim_{Q \to \infty} \frac{1}{Q} \sum_{\alpha=1}^{Q} \langle f \rangle_\alpha. \quad (16)$$

2. Probability distribution for average within a sample

On the other hand, we can view the numbers $x = \langle f \rangle_\alpha$ as random variables according to the distribution

$$s(x) = \frac{1}{(2h)^K} \int_{-h}^{h} dh_1 \cdots \int_{-h}^{h} dh_K$$

$$\times \delta\left(x - \int_0^1 dr \, p(r; h_1, \ldots, h_K) f(r)\right), \quad (17)$$

where $p(r; h_1, \ldots, h_K) = p_\alpha$ is the probability distribution within a system with local disorder fields $h_1, \ldots, h_K$ forming the disorder realization α. Thus, the disorder-averaged expectation value of $f(r)$ can be formulated as

$$\langle f \rangle_s = \int dx \, s(x) x = \lim_{Q \to \infty} \frac{1}{Q} \sum_{\alpha=1}^{Q} \langle f \rangle_\alpha = \langle f \rangle_p, \quad (18)$$

where the integration goes over all values of $x = f(r)$ for $r \in [0, 1]$. The distribution $s(x)$ does not, in general, coincide with $p(r)$ even for $x = f(r) = r$. Moreover $s(x)$ will of course have a dependence on the function f, which we, however, shall suppress in the notation.

The finite average

$$\bar{f} = \frac{1}{Q} \sum_{\alpha=1}^{Q} \langle f \rangle_\alpha \approx \langle f \rangle_s, \quad (19)$$

is, again for appropriately large Q, an approximation to the expression (18). On the other hand, it is a sum of stochastically

independent (and therefore uncorrelated) random variables with identical probability distribution, so that the resulting joint distribution is

$$\pi(x_1, \ldots, x_Q) = \prod_{\alpha=1}^{Q} s(x_\alpha). \tag{20}$$

Thus, the expectation value of $\bar{f}$ is

$$\langle \bar{f} \rangle_\pi = \frac{1}{Q} \sum_{\alpha=1}^{Q} \langle f \rangle_s = \langle f \rangle_s. \tag{21}$$

3. Sample-to-sample variance

For the variance pertaining to the expectation value (21) one finds

$$\left\langle (\bar{f} - \langle f \rangle_s)^2 \right\rangle_\pi = \sum_{\alpha,\beta=1}^{Q} \frac{\langle (\langle f \rangle_\alpha - \langle f \rangle_s)(\langle f \rangle_\beta - \langle f \rangle_s) \rangle_\pi}{Q^2}$$

$$= \frac{1}{Q^2} \sum_{\alpha=1}^{Q} \left\langle (\langle f \rangle_\alpha - \langle f \rangle_s)^2 \right\rangle_s = \frac{(\Delta_s f)^2}{Q} \tag{22}$$

with

$$(\Delta_s f)^2 = \langle (f - \langle f \rangle_s)^2 \rangle_s$$

$$= \lim_{Q \to \infty} \frac{1}{Q} \sum_{\alpha=1}^{Q} (\langle f \rangle_\alpha - \langle f \rangle_s)^2. \tag{23}$$

Therefore, the fluctuations of the finite average (18) around its expectation value (21) are characterized by the standard deviation

$$\Delta_\pi \bar{f} = \sqrt{\left\langle (\bar{f} - \langle f \rangle_s)^2 \right\rangle_\pi} = \frac{\Delta_s f}{\sqrt{Q}} \tag{24}$$

and shows the familiar decay $\propto 1/\sqrt{Q}$. This result follows of course also from the Lindeberg-Levy central limit theorem applied to the sum (19) of random variables. An approximate expression for the variance (23) is

$$(\Delta_s f)^2 \approx \frac{1}{Q} \sum_{\alpha=1}^{Q} (\langle f \rangle_\alpha - \bar{f})^2, \quad Q \gg 1. \tag{25}$$

Note that the variance (23) also occurs as a contribution to the variance of $f(r)$ calculated from the disorder-averaged probability distribution (14),

$$(\Delta_p f)^2 = \int_0^1 dr \, p(r)(f(r) - \langle f \rangle_p)^2 \tag{26}$$

$$= \lim_{Q \to \infty} \frac{1}{Q} \sum_{\alpha=1}^{Q} (\Delta_\alpha f)^2 + (\Delta_s f)^2, \tag{27}$$

as derived in Appendix A. Hence, the variance (26) with respect to the averaged probability distribution (14) is the average of all variances within the disorder realizations around their individual expectation value of f, plus the variance (23) describing the fluctuations of these expectation values

around their mean. An approximate expression for the above result is

$$(\Delta_p f)^2 \approx \frac{1}{Q} \sum_{\alpha=1}^{Q} \int_0^1 dr \, p_\alpha(r)[f(r) - \bar{f}]^2 \tag{28}$$

$$= \frac{1}{Q} \sum_{\alpha=1}^{Q} (\Delta_\alpha f)^2 + \frac{1}{Q} \sum_{\alpha=1}^{Q} (\langle f \rangle_\alpha - \bar{f})^2, \tag{29}$$

where again $Q \gg 1$.

4. Variance of the variance

Let us now analyze the statistical fluctuations of the right-hand side of the approximate quantity (25) for finite Q and define

$$\bar{g} := \frac{1}{Q} \sum_{\alpha=1}^{Q} (\langle f \rangle_\alpha - \bar{f})^2 = \frac{1}{Q} \sum_{\alpha=1}^{Q} \left(\langle f \rangle_\alpha^2 - \bar{f}^2 \right). \tag{30}$$

An important difference between the above expression and the quantity (19) is that above the summands depend, again via Eq. (19), on all expectation values $\langle f \rangle_\alpha$, $\alpha \in \{1, \ldots, Q\}$, and are therefore distributed according to the joint probability distribution (20). The expectation value of the random variable (30) with respect to the latter distribution is (Appendix B)

$$\langle \bar{g} \rangle_\pi = \frac{Q-1}{Q} (\Delta_s f)^2, \tag{31}$$

which approaches the variance (23) for large Q. Note also that, in contrast to Eq. (18), it holds

$$\langle f^2 \rangle_s = \int dx \, s(x) x^2 = \lim_{Q \to \infty} \frac{1}{Q} \sum_{\alpha=1}^{Q} \langle f \rangle_\alpha^2 \neq \langle f^2 \rangle_p. \tag{32}$$

It is now straightforward to establish that (Appendix B), analogously as in Eq. (22),

$$(\Delta_\pi \bar{g})^2 = \frac{(\Delta_s f^2)^2}{Q} + O\left(\frac{1}{Q^2} \right), \tag{33}$$

where

$$(\Delta_s f^2)^2 = (\Delta_s [(\Delta_s f)^2])^2. \tag{34}$$

5. Consecutive-gap ratio

In what follows we will be mainly concerned with the function $f(r) = r$ where we have

$$(\Delta_s r)^2 = \lim_{Q \to \infty} \frac{1}{Q} \sum_{\alpha=1}^{Q} (\langle r \rangle_\alpha - \langle r \rangle_s)^2$$

$$= \lim_{Q \to \infty} \frac{1}{Q} \sum_{\alpha=1}^{Q} \left(\langle r \rangle_\alpha^2 - \langle r \rangle_s^2 \right) \tag{35}$$

with

$$\langle r \rangle_s = \int_0^1 dx \, s(x) x = \lim_{Q \to \infty} \frac{1}{Q} \sum_{\alpha=1}^{Q} \langle r \rangle_\alpha = \langle r \rangle_p, \tag{36}$$

where $s(x)$ is, in accordance with Eq. (17), the probability distribution for the random variable $x = \langle r \rangle_\alpha$. Finally, as seen
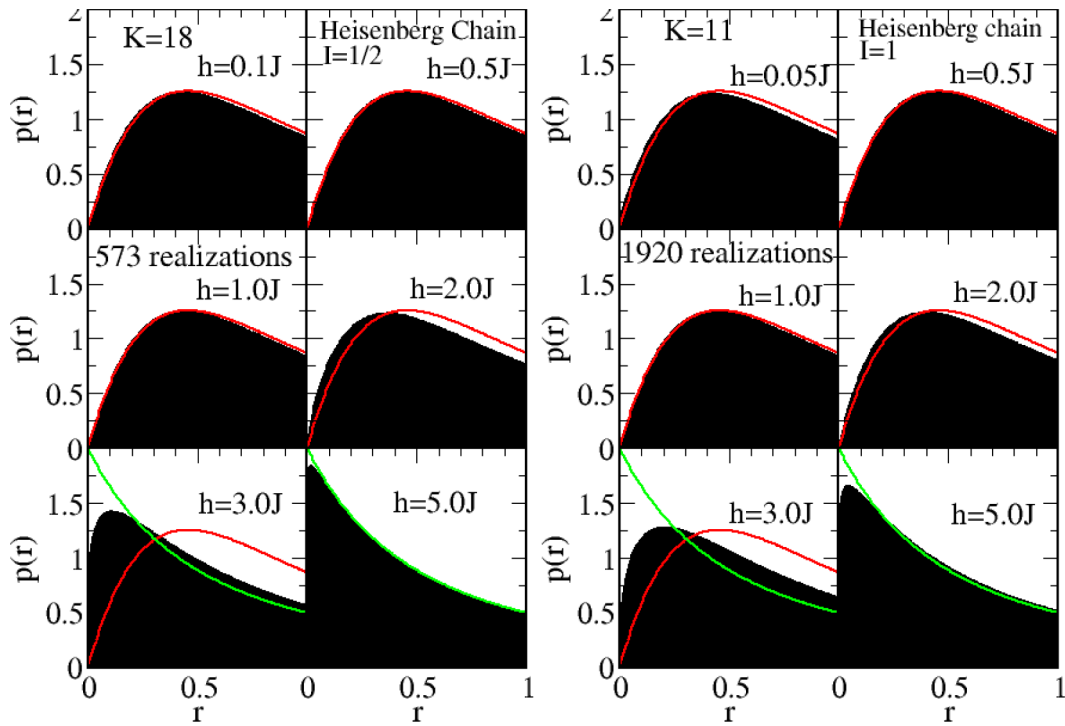
FIG. 1. The probability distribution (15) for the consecutive-gap ratio r of a Heisenberg chain ($A = 0$) of $K = 18$ spins of length $I = 1/2$ (left) and of $K = 11$ spins of length $I = 1$ (right) for different disorder strength h obtained from exact-diagonalization data. At small disorder the system is ergodic and well described by the distribution (4) (red), while with increasing h a transition to the Poisson-type distribution (3) (green) sets in.

in Eq. (34), the variance of the variance (35) is determined by

$$(\Delta_s r^2)^2 = \langle r^4 \rangle_s - \langle r^2 \rangle_s^2 = \langle (r^2 - \langle r^2 \rangle_s)^2 \rangle_s$$
$$= (\Delta_s[(\Delta_s r)^2])^2. \quad (37)$$

III. NUMERICAL RESULTS

The Hamiltonian (1) obviously conserves the z component of the total spin,

$$\vec{J} = \vec{S} + \sum_{i=1}^{K} \vec{I}_i, \quad [H, J^z] = 0. \quad (38)$$

Thus, in order to apply random matrix theory, the spectra of each invariant subspace of J^z have to be analyzed separately [46]. In this section we present accumulated exact-diagonalization data from a separate evaluation of all subspaces of J^z except for the four subspaces of smallest dimension where $|J^z|$ is maximal or differs from its maximal value by 1. The number of disorder realizations varies, depending on system size, between several hundreds and 2×10^5.

A. Heisenberg chain

For $A = 0$ the central spin $\vec{S}$ becomes obsolete, and for $I = 1/2$ and vanishing disorder $h = 0$ the resulting Heisenberg chain is integrable via the Bethe ansatz [49]. However, this is a rather isolated point in the phase diagram as seen in Fig. 1 showing the disorder-averaged probability distribution (15) obtained from exact-diagonalization data of the Heisenberg

chain with spin lengths $I = 1/2$ and $I = 1$ at different disorder strengths. For even small disorder such as $h = 0.1J$ the system shows ergodic statistics (4) while upon increasing h it changes to the Poisson-type distribution (3). This transition occurs for both spin lengths at about the same disorder strength, which is a consequence of the scaling factor $2S = 2I$ in the disorder term of the Hamiltonian (1). The fact that both spin lengths show such a similar behavior is consistent with the assumption that the system smoothly approaches its classical limit and therefor corroborates semiclassical approaches to many-body localization in spin chains [28,50]. In Fig. 2 we show the expectation value $\langle r \rangle_p = \langle r \rangle_s$ as a function of disorder strength for Heisenberg chains of different sizes along with the standard deviation $\Delta_p r$ (top panels). The data shows a transition between the ergodic phase at small h characterized by Eqs. (9) and (11) to the values (5) and (7) of the many-body localized phase. The bottom panels display the sample-to-sample standard deviation $\Delta_s r$ according to Eqs. (25) and (35). As seen from the figures, $\Delta_s r$ amounts only to about 10% of $\Delta_p r$, which demonstrates via Eq. (27) that $(\Delta_s r)^2$ is only a tiny contribution to the variance $(\Delta_p r)^2$. On the other hand, $\Delta_s r$ shows a pronounced maximum $(\Delta_s r)_{\max}$ which grows rapidly with system size, as displayed in the insets of the lower panels. Moreover, in close vicinity to the corresponding position $h = h_{\max}$, $\langle r \rangle_s$ has an inflection point at $h = h_{\inf}$. In Fig. 3 we have plotted both disorder strengths for $I \in \{1/2, 1\}$ as functions of systems size K, which shows that both quantities seem to converge to a common value for large K. Thus, the expectation value $\langle r \rangle_s$ and the standard deviation $\Delta_s r$ show as a function of disorder strength typical features of a phase
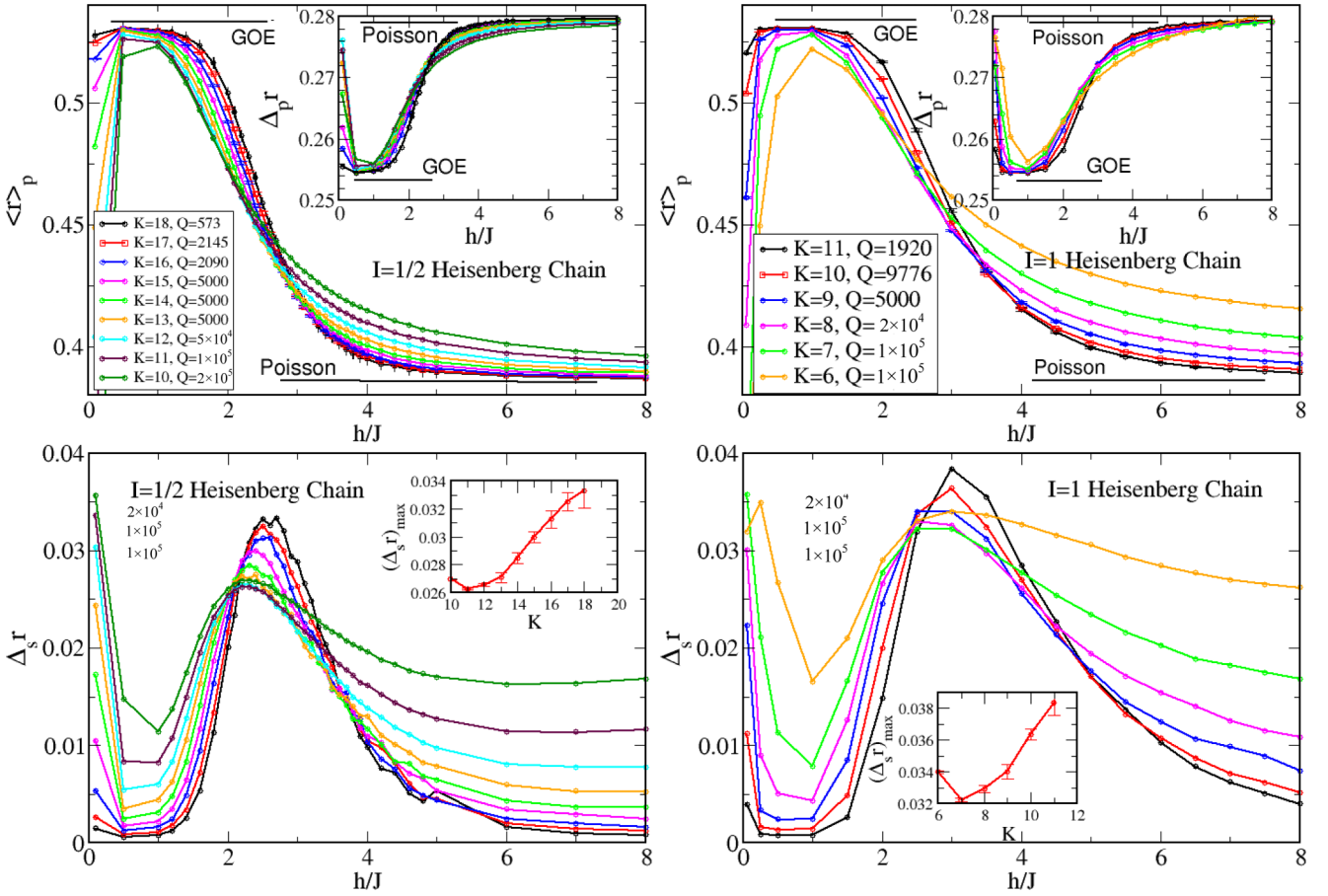
FIG. 2. Top panels: The expectation value $\langle r \rangle_p$ as a function of disorder strength in Heisenberg chains of spin length $I = 1/2$ (left) and $I = 1$ (right) for various system sizes and pertaining to numbers of disorder realizations. The error bars are determined by Eqs. (24) and (25). Inset: The standard deviation $\Delta_p r$ as a function of disorder strength. The horizontal lines indicate the expected values for GOE and Poissonian statistics as given in Eqs. (5)–(11). Bottom panels: The standard deviation $\Delta_s r$ according to Eq. (25) for the same parameters as in the top panels. For a more detailed view on the data at large system sizes see also Fig. 4. The insets show the maximum of the standard deviation as a function of system size where the error bars follow Eqs. (34) and (37).

transition with the former quantity playing the role of an order parameter. The crossing points of the data shown in the top
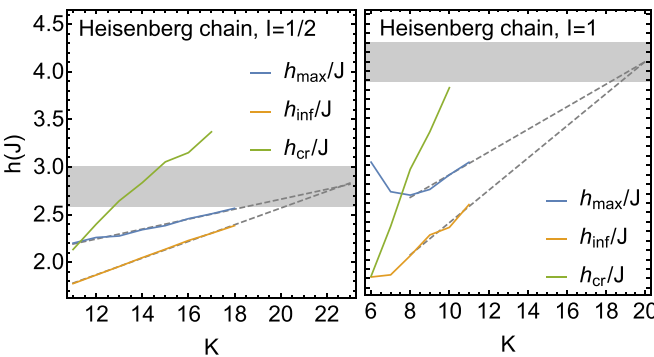

FIG. 3. Finite-size transition data for the Heisenberg chain of spin length $I = 1/2$ (left) and $I = 1$ (right). The panels show as a function of system size K the position $h = h_{\max}$ of $(\Delta_s r)_{\max}$, the position $h = h_{\inf}$ of the inflection point of $\langle r \rangle_s$, and the crossing point $h = h_{cr}(K)$ of two curves of the latter quantity with consecutive system sizes K and $K + 1$. The dashed lines are linear fits to $h_{\max}$ and $h_{\inf}$, and the shaded regions estimate the transition where $h_{\max} \approx h_{\inf}$.

panels of Fig. 2 are also often considered as indications for a phase transition. Therefore, following Refs. [14,51], we also plot in Fig. 3 the positions $h = h_{cr}(K)$ where two curves of $\langle r \rangle_s$ with consecutive system sizes K and $K + 1$ cross. This data set clearly deviates from $h_{\max}$, $h_{\inf}$ and grows to larger disorder strengths, an observation known as the "drifting of the critical disorder strength" with system size [14,27]. It is an interesting speculation whether $h_{\max} \approx h_{\inf}$ and h_{cr} correspond, for large systems, to two distinct transitions occurring in the same systems.

For the finite-size data depicted in Fig. 3 we estimate the transition point to $h_{\max} \approx h_{\inf} \approx 2.6J \ldots 3.0J$ for spin length $I = 1/2$, and $h_{\max} \approx h_{\inf} \approx 4.0J \ldots 4.5J$ for $I = 1$. These values for the critical disorder strength for the transition from the ergodic to the many-body localized phase are somewhat smaller than those reported in other works [14,16,20,33,36], which favor, for $I = 1/2$, values of $h/J \approx 4$ or larger. However, some of these works [14,16,33] concentrate on chains with an even number of spins and the subspace with total spin $J^z = 0$, whereas here we also take into account odd numbers of spins and all subspaces except for those with $|J^z| \in \{IK, IK - 1\}$. Moreover, we introduce a new criterion
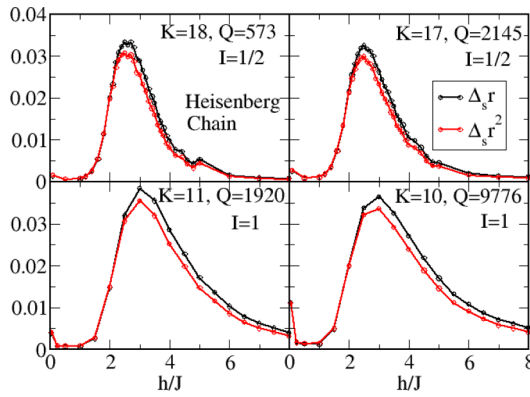
FIG. 4. The sample-to-sample standard deviation $\Delta_s r$ along with the square root of variance of the variance (37) as a function of disorder strength h for Heisenberg chains of spin length $I = 1/2$ (top panels) and $I = 1$ (bottom panels). The data sets are remarkably close to each other, in particular at small disorder strength h.

to locate the transition given by the position of $(\Delta_s r)_{\max}$. On the other hand, the fact that the transition occurs for $I = 1$ at larger disorder strength compared to $I = 1/2$ is consistent with observations made in Ref. [41]. Figure 4 shows the standard deviation $\Delta_s r$ along with the square root of "variance of the variance" (37) as a function of disorder strength for both spin lengths $I = 1/2$ and $I = 1$. Remarkably, both quantities are very close to each other, especially at small disorder strength h. This observation should be taken as an indication that the underlying probability distribution $s(x)$ is rather narrow since both quantities become strictly

equal, $\Delta_s r = \Delta_s r^2 = 0$, for a δ-type distribution. This conjecture is confirmed by the data of Fig. 5 which displays the probability distribution (17) for the realization-specific average $\langle r \rangle_\alpha$ with the disorder strengths being the same as in Fig. 1. The probability distribution is much narrower than the distribution $p(r)$ and broadens significantly in the transition region. The latter result is similar to an obsevation by Pal and Huse [14] who found near the transition a maximum in the width of the probability distribution of a long-ranged spin correlator. We also note that a closer analysis of the data of the lower panels of Fig. 4 suggests that $\Delta_s r$ extrapolates to zero for $K \to \infty$ deep in the ergodic phase ($h/J \approx 1$) as well as deep in the many-body localized phase ($h/J \gtrsim 6$). This would mean that the probability distribution (17) would develop into a δ function in this limit and the above range of disorder strengths, which is consistent with the data of Fig. 5. Note that the statement $\lim_{K \to \infty} \Delta_s r = 0$ implies, according to Eq. (27), that the variance $(\Delta_p r)^2$ is entirely given by the averaged variances within the individual disorder realizations.

B. Central spin model

The central spin model is defined by putting $J = 0$ in the Hamiltonian (1). This system is also integrable via an appropriate Bethe ansatz and known as the Gaudin model [52,53]. Compared to the Heisenberg chain, the coupling to the central spin provides an alternative mechanism of introducing interaction among the bath spins, which are subject to a random magnetic field.

Figure 6 shows data analogous to Fig. 1 now for central spin models of spin length $S = I = 1/2$ and $S = I = 1$. For
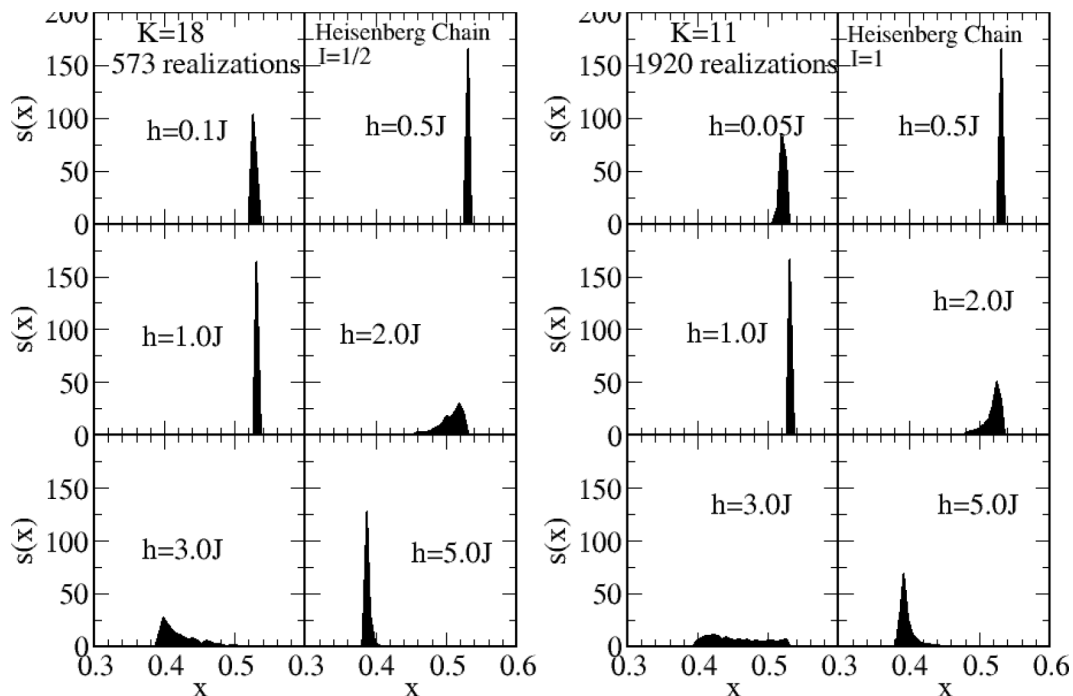

FIG. 5. The probability distribution (17) for the realization-specific average $\langle r \rangle_\alpha$ for disordered Heisenberg chains of spin length $I = 1/2$ (left) and $I = 1$ (right). The disorder strengths h in both panels are the same as in Fig. 1.
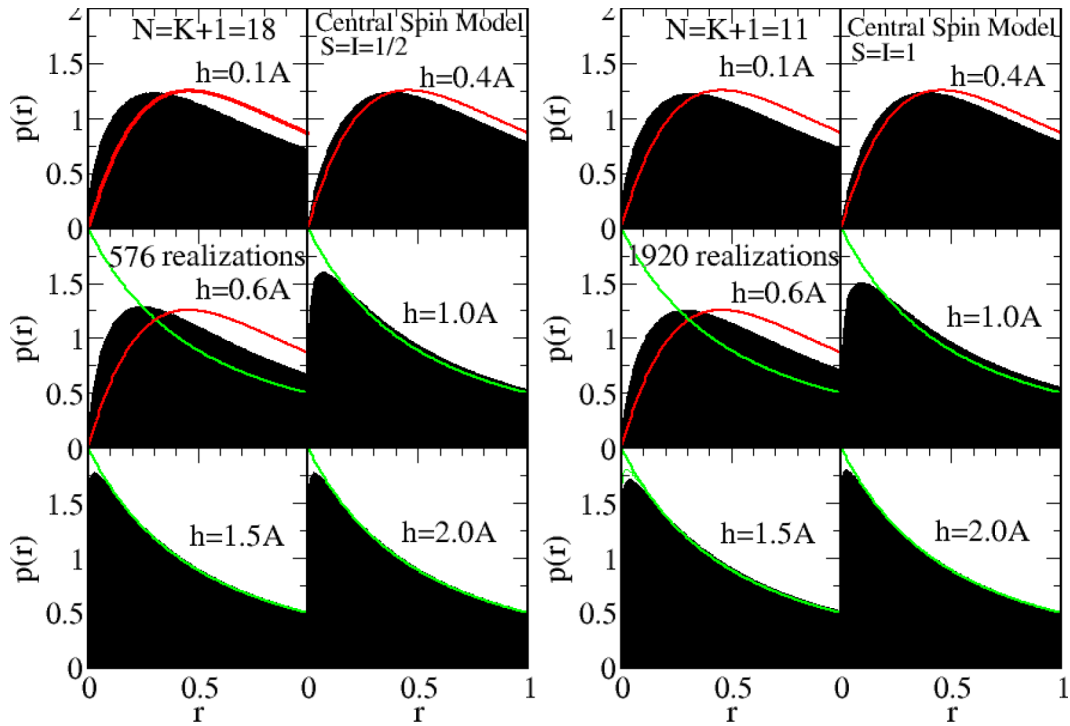
FIG. 6. The probability distribution (15) for the consecutive-gap ratio r of a central spin model ($J = 0$) of $N = K + 1 = 11$ spins of length $S = I = 1/2$ (left) and of $N = K + 1 = 10$ spins of length $S = I = 1$ (right) for different disorder strength h. Similarly as for the Heisenberg chain, the data follows for small but finite disorder approximately GOE distribution (4) (red), while with increasing h a transition to the Poisson-type distribution (3) (green) sets in.

small disorder, the system clearly deviates from the Poisson-type distribution (3) and shows level repulsion. However, differently from the case of the Heisenberg chain, the level statistics do not fully reach the Gaussian orthogonal ensemble but change back before to an integrable or many-body localized phase. Figure 7 displays data for the central spin model analogous to Fig. 2 for the Heisenberg chain. Comparing the top panels of both figures suggests a transition from the (approximately) ergodic to the many-body localized phase at the inflection point $h = h_{\text{inf}} \lesssim 1$, which is consistent with the findings of Ref. [45] for $A, h \gg J$. Here the fact that the transition occurs at about the same disorder strength for different system sizes depends on the scaling factor $1/K$ in front of the second term in the Hamiltonian (1). Also the sample-to-sample standard deviation $\Delta_s r$ plotted in the bottom panels of Fig. 7 behaves similarly as for the Heisenberg chain: For large enough system sizes this quantity develops a maximum $(\Delta_s r)_{\text{max}}$ near $h = h_{\text{inf}}$ whose value increases monotonically with system size, as shown in the insets. Thus, we have qualitatively the same situation as for the Heisenberg chain. Moreover, as can be seen in Fig. 8, the square root of the variance of the variance (37) closely follows, similarly as for the Heisenberg chain, the standard deviation $\Delta_s r$ as a function of disorder strength for both spin lengths $I = 1/2$ and $I = 1$. This is consistent with the probability distribution (17) for the realization-specific average $\langle r \rangle_\alpha$ shown in Fig. 9. As already seen in the case of the Heisenberg chain, the probability distribution is much narrower than the distribution $p(r)$ and becomes significantly broader in the transition region.

IV. SUMMARY AND OUTLOOK

We have compared the transitions between ergodic and many-body localized phases in disodered Heisenberg chains as well as central spin models composed of spins of length 1/2 and 1. A useful tool we introduce is the sample-to-sample standard deviation $\Delta_s r$ of the expectation value $\langle r \rangle_\alpha$ of the consecutive-gap ratio in an individual disorder realization (sample) α. This quantity assumes, for both types of systems and spin lengths, a maximum as a function of disorder strength, accompanied by an inflection point of $\langle r \rangle$. These are typical features of a phase transition where the latter quantity plays the role of an order parameter. The critical disorder strength deduced from these observations turns out to be smaller than those reported in the recent literature.

Further information about the transitions is contained in the probability distribution of the expectation values within a given disorder realization. We expect the study of this probability distribution and its moments to be a useful tool in the investigation of phenomena related to many-body localization also in other systems.
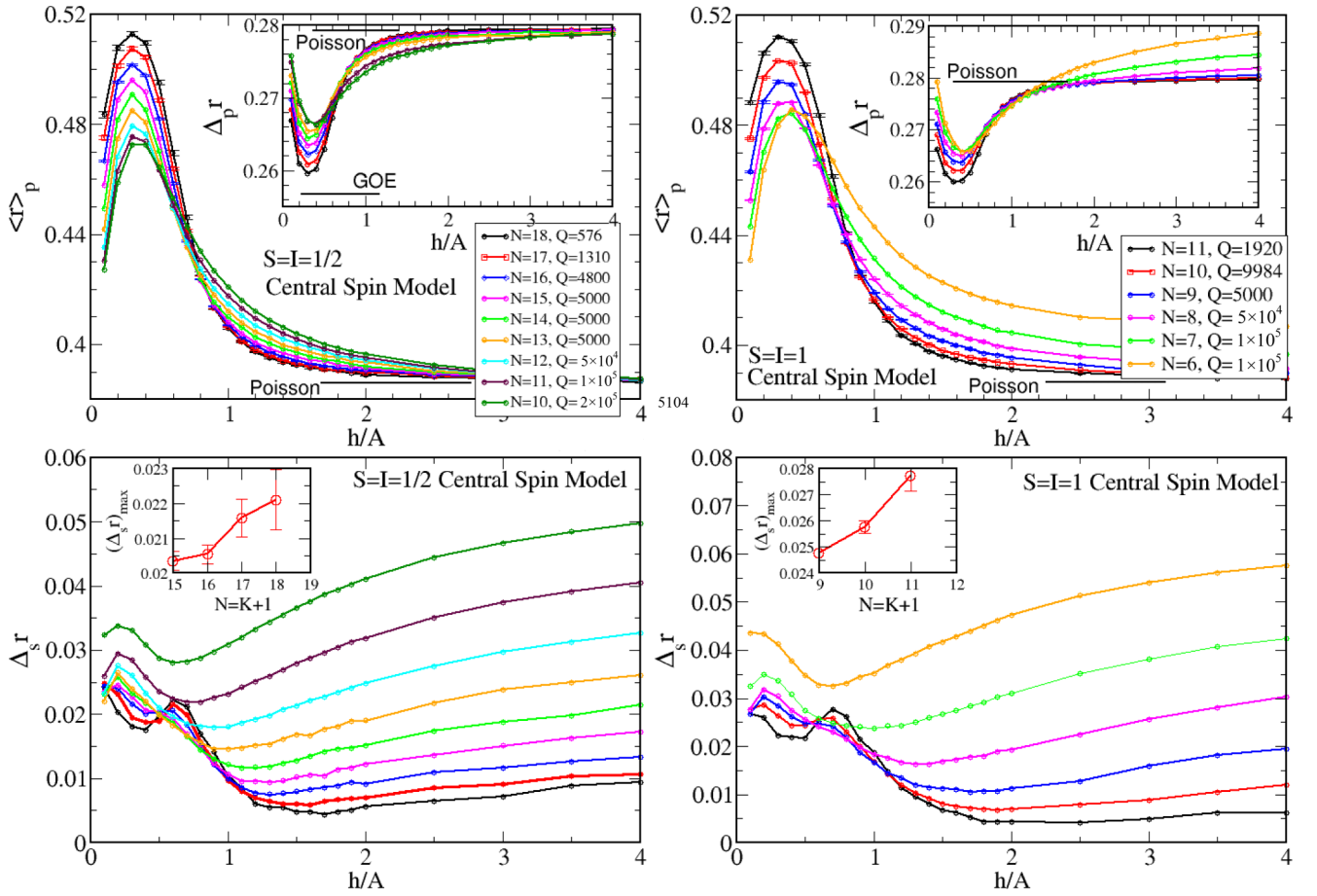
FIG. 7. Top panels: The expectation value $\langle r \rangle_p$ as a function of disorder strength in central spin models of spin length $S = I = 1/2$ (left) and $S = I = 1$ (right) for various system sizes and pertaining to numbers of disorder realizations. The error bars are determined by Eqs. (24) and (25). Inset: The standard deviation $\Delta_p r$ as a function of disorder strength. The horizontal lines indicate the expected values for GOE and Poissonian statistics as given in Eqs. (5)–(11). Bottom panels: The standard deviation $\Delta_s r$ according to Eq. (25) for the same parameters as in the top panels. For a more detailed view on the data at large system sizes see also Fig. 8. The insets show the maximum of the standard deviation as a function of system size.

APPENDIX A: VARIANCE OF f FROM DISORDER-AVERAGED PROBABILITY DISTRIBUTION

The variance calculated from the disorder-averaged probability distribution is given by

$$(\Delta_p f)^2 = \int_0^1 dr\, p(r)[f(r) - \langle f \rangle_p]^2 \tag{A1}$$

$$= \lim_{Q \to \infty} \frac{1}{Q} \sum_{\alpha=1}^{Q} \int_0^1 dr\, p_\alpha(r)(f(r) - \langle f \rangle_p)^2$$

$$= \lim_{Q \to \infty} \frac{1}{Q} \sum_{\alpha=1}^{Q} \left(\langle f^2 \rangle_\alpha - \langle f \rangle_\alpha^2 \right)$$

$$+ \lim_{Q \to \infty} \frac{1}{Q} \sum_{\alpha=1}^{Q} \left(\langle f \rangle_\alpha^2 - \langle f \rangle_p^2 \right)$$

$$= \lim_{Q \to \infty} \frac{1}{Q} \sum_{\alpha=1}^{Q} (\Delta_\alpha f)^2 + (\Delta_s f)^2. \tag{A2}$$
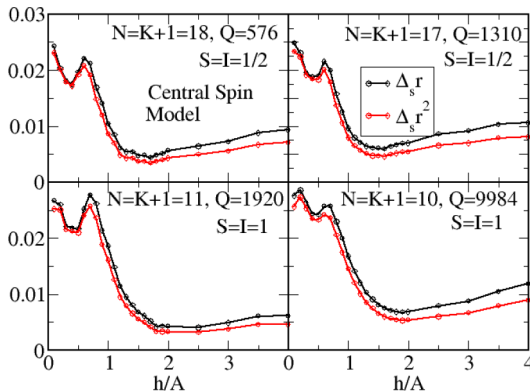

FIG. 8. The sample-to-sample standard deviation $\Delta_s r$ along with the square root of variance of the variance (37) as a function of disorder strength h for central spin models of spin length $S = I = 1/2$ (top panels) and $S = I = 1$ (bottom panels).
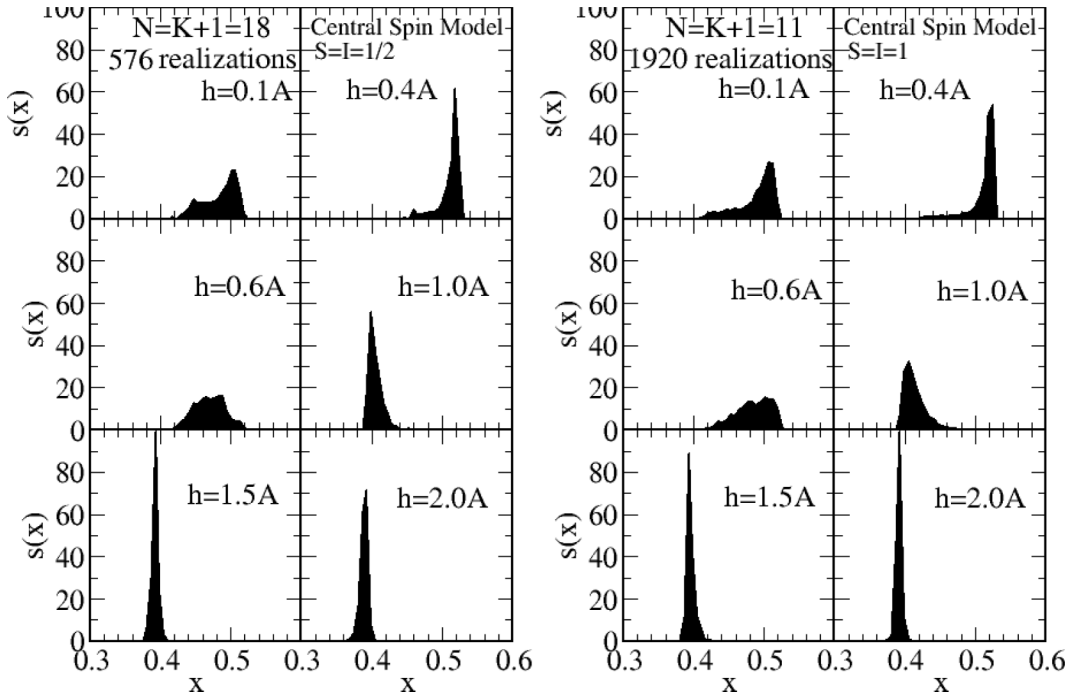
FIG. 9. The probability distribution (17) for the realization-specific average $\langle r \rangle_\alpha$ for disordered central spin systems of spin length $S = I = 1/2$ (left) and $S = I = 1$ (right). The disorder strengths h in both panels are the same as in Fig. 6.

APPENDIX B: VARIANCE OF THE VARIANCE

The expectation value $\langle \bar{g} \rangle_\pi$ is given by

$$\langle \bar{g} \rangle_\pi = \frac{1}{Q}\left(\sum_{\alpha=1}^{Q} \langle \langle f \rangle_\alpha^2 \rangle_\pi - \frac{1}{Q} \sum_{\alpha,\beta=1}^{Q} \langle \langle f \rangle_\alpha \langle f \rangle_\beta \rangle_\pi \right)$$

$$= \frac{Q-1}{Q}\left(\langle f^2 \rangle_s - \langle f \rangle_s^2 \right) = \frac{Q-1}{Q}(\Delta_s f)^2. \quad (B1)$$

Using

$$\left\langle (\langle f \rangle_\alpha^2 - \bar{f}^2 - \langle \bar{g} \rangle_\pi)(\langle f \rangle_\beta^2 - \bar{f}^2 - \langle \bar{g} \rangle_\pi) \right\rangle_\pi$$

$$= \delta_{\alpha\beta}\left(\langle f^4 \rangle_s - \langle f^2 \rangle_s^2 \right) + O\left(\frac{1}{Q}\right), \quad (B2)$$

it follows that

$$(\Delta_\pi \bar{g})^2 = \sum_{\alpha,\beta=1}^{Q} \frac{\left\langle (\langle f \rangle_\alpha^2 - \bar{f}^2 - \langle \bar{g} \rangle_\pi)(\langle f \rangle_\beta^2 - \bar{f}^2 - \langle \bar{g} \rangle_\pi) \right\rangle_\pi}{Q^2}$$

$$= \frac{(\Delta_s f^2)^2}{Q} + O\left(\frac{1}{Q^2}\right), \quad (B3)$$

where

$$(\Delta_s f^2)^2 = \langle f^4 \rangle_s - \langle f^2 \rangle_s^2 = \langle (f^2 - \langle f^2 \rangle_s)^2 \rangle_s$$

$$= (\Delta_s[(\Delta_s f)^2])^2. \quad (B4)$$

[1] R. Nandkishore and D. A. Huse, Annu. Rev. Condens. Matter Phys. **6**, 15 (2015).

[2] E. Altman and R. Vosk, Annu. Rev. Condens. Matter Phys. **6**, 383 (2015).

[3] J. Z. Imbrie, V. Ros, and A. Scardicchio, Ann. Phys. (Berlin) **529**, 1600278 (2017).

[4] K. Agarwal, E. Altman, E. Demler, S. Gopalakrishnan, D. A. Huse, and M. Knap, Ann. Phys. (Berlin) **529**, 1600326 (2017).

[5] D. J. Luitz and Y. Bar Lev, Ann. Phys. (Berlin) **529**, 1600350 (2017).

[6] A. Haldar and A. Das, Ann. Phys. (Berlin) **529**, 1600333 (2017).

[7] D. A. Abanin and Z. Papic, Ann. Phys. (Berlin) **529**, 1700169 (2017).

[8] D. A. Abanin, E. Altman, I. Bloch, and M. Serbyn, Rev. Mod. Phys. **91**, 021001 (2019).

[9] J. M. Deutsch, Phys. Rev. A **43**, 2046 (1991).

[10] M. Srednicki, Phys. Rev. E **50**, 888 (1994).

[11] P. W. Anderson, Phys. Rev. **109**, 1492 (1958).

[12] F. Evers and A. D. Mirlin, Rev. Mod. Phys. **80**, 1355 (2008).

[13] L. F. Santos, G. Rigolin, and C. O. Escobar, Phys. Rev. A **69**, 042304 (2004).

[14] A. Pal and D. A. Huse, Phys. Rev. B **82**, 174411 (2010).

[15] J. H. Bardarson, F. Pollmann, and J. E. Moore, Phys. Rev. Lett. **109**, 017202 (2012).

[16] D. J. Luitz, N. Laflorencie, and F. Alet, Phys. Rev. B **91**, 081103(R) (2015).

[17] A. Chandran, I. H. Kim, G. Vidal, and D. A. Abanin, Phys. Rev. B **91**, 085425 (2015).

[18] K. Agarwal, S. Gopalakrishnan, M. Knap, M. Muller, and E. Demler, Phys. Rev. Lett. **114**, 160401 (2015).

[19] E. Baygan, S. P. Lim, and D. N. Sheng, Phys. Rev. B **92**, 195153 (2015).

[20] T. Devakul and R. R. P. Singh, Phys. Rev. Lett. **115**, 187201 (2015).

[21] D. J. Luitz, N. Laflorencie, and F. Alet, Phys. Rev. B **93**, 060201(R) (2016).

[22] D. J. Luitz, Phys. Rev. B **93**, 134201 (2016).

[23] S. D. Geraedts, R. M. Nandkishore, and N. Regnault, Phys. Rev. B **93**, 174202 (2016).

[24] V. Khemani, A. Lazarides, R. Moessner, and S. L. Sondhi, Phys. Rev. Lett. **116**, 250401 (2016).

[25] S. P. Lim and D. N. Sheng, Phys. Rev. B **94**, 045111 (2016).

[26] M. Serbyn, A. A. Michailidis, D. A. Abanin, and Z. Papic, Phys. Rev. Lett. **117**, 160601 (2016).

[27] T. Enss, F. Andraschko, and J. Sirker, Phys. Rev. B **95**, 045121 (2017).

[28] O. L. Acevedo, A. Safavi-Naini, J. Schachenmayer, M. L. Wall, R. Nandkishore, and A. M. Rey, Phys. Rev. A **96**, 033604 (2017).

[29] V. Khemani, D. N. Sheng, and D. A. Huse, Phys. Rev. Lett. **119**, 075702 (2017).

[30] Jaime L. C.da C. Filho, A. Saguia, L. F. Santos, and M. S. Sarandy, Phys. Rev. B **96**, 014204 (2017).

[31] S. D. Geraedts, N. Regnault, and R. M. Nandkishore, New J. Phys. **19**, 113021 (2017).

[32] K. Xu, J.-J. Chen, Y. Zeng, Y.-R. Zhang, C. Song, W. Liu, Q. Guo, P. Zhang, D. Xu, H. Deng, K. Huang, H. Wang, X. Zhu, D. Zheng, and H. Fan, Phys. Rev. Lett. **120**, 050507 (2018).

[33] E. V. H. Doggen, F. Schindler, K. S. Tikhonov, A. D. Mirlin, T. Neupert, D. G. Polyakov, and I. V. Gornyi, Phys. Rev. B **98**, 174202 (2018).

[34] J. Suntajs, J. Bonca, T. Prosen, and L. Vidmar, Phys. Rev. E **102**, 062144 (2020).

[35] R. K. Panda, A. Scardicchio, M. Schulz, S. R. Taylor, and M. Znidaric, Europhys. Lett. **128**, 67003 (2020).

[36] T. Chanda, P. Sierant, and J. Zakrzewski, Phys. Rev. B **101**, 035148 (2020).

[37] J. Suntajs, J. Bonca, T. Prosen, and L. Vidmar, Phys. Rev. B **102**, 064207 (2020).

[38] N. Laflorencie, G. Lemarie, and N. Mace, Phys. Rev. Res. **2**, 042033(R) (2020).

[39] P. Sierant, M. Lewenstein, and J. Zakrzewski, Phys. Rev. Lett. **125**, 156601 (2020).

[40] S. Dhara, A. Hamma, and E. R. Mucciolo, Phys. Rev. B **102**, 045140 (2020).

[41] J. Richter, D. Schubert, and R. Steinigeweg, Phys. Rev. Res. **2**, 013130 (2020).

[42] Q. Guo, C. Cheng, Z.-H. Sun, Z. Song, H. Li, Z. Wang, W. Ren, H. Dong, D. Zheng, Y.-R-. Zhang, R. Mondaini, H. Fan, and H. Wang, Nat. Phys. **17**, 234 (2021).

[43] T. Chanda, P. Sierant, and J. Zakrzewski, Phys. Rev. Res. **2**, 032045(R) (2020).

[44] R. E. Throckmorton and S. Das Sarma, Phys. Rev. B **103**, 165431 (2021).

[45] D. Hetterich, N. Y. Yao, M. Serbyn, F. Pollmann, and B. Trauzettel, Phys. Rev. B **98**, 161122(R) (2018).

[46] T. Guhr, A. Muller-Groeling, and H. A. Weidenmuller, Phys. Rep. **299**, 189 (1998).

[47] V. Oganesyan and D. A. Huse, Phys. Rev. B **75**, 155111 (2007).

[48] Y. Y. Atas, E. Bogomolny, O. Giraud, and G. Roux, Phys. Rev. Lett. **110**, 084101 (2013).

[49] H. Bethe, Z. Phys. A **71**, 205 (1931).

[50] B. Craps, M. De Clerck, D. Janssens, V. Luyten, and C. Rabideau, Phys. Rev. B **101**, 174313 (2020).

[51] K. S. Tikhonov, A. D. Mirlin, and M. A. Skvortsov, Phys. Rev. B **94**, 220203(R) (2016).

[52] M. Gaudin, J. Phys. (Paris) **37**, 1087 (1976).

[53] B. Erbe and J. Schliemann, Phys. Rev. Lett. **105**, 177602 (2010).